Influence of reaction parameters on the synthesis of surfactant-assisted tin oxide nanoparticles

Muhammad Akhyar FARRUKH[1]**, Prisca TAN**[2]** and Rohana ADNAN**[2,*]

[1]*Department of Chemistry, GC University Lahore, 54000 Lahore-PAKISTAN*

e-mail: akhyar100@gmail.com

[2]*School of Chemical Sciences, Universiti Sains Malaysia, 11800 Penang-MALAYSIA*

e-mail: r_adnan@usm.my

Tin oxide nanoparticles were synthesized via hydrothermal method using a non-ionic surfactant, oleyl amine (OLM), in the presence of urea. The reactions were carried out at different calcination temperatures and varying concentrations of surfactant and urea. The effect of these reaction parameters on the particles' size, distribution, surface area, and the average pore diameter were investigated using X-ray diffraction analysis, transmission electron microscopy, scanning electron microscopy, energy dispersive X-ray analysis, thermogravimetric analysis, Brunauer-Emmett-Teller method, and Fourier transform infrared spectroscopy. Larger tin oxide nanoparticles were obtained with higher concentrations of urea. At the optimum experimental conditions, tin oxide nanoparticles with mean particle size of 9.92 nm and surface area of 31.82 m^2 g^{-1} were obtained. Particle size further decreased to 5.36 nm with the addition of surfactant having a concentration below CMC. Elimination of surfactant from tin-surfactant composites after calcination yielded mesoporous particles but the increase in calcination temperature resulted in larger and highly aggregated tin oxide particles.

Key Words: Nanoparticles, tin oxide, hydrothermal, surfactant, reaction parameters, microscopy

Introduction

Tin oxide is a wide band gap n-type semiconductor with many potential applications such as catalysts for oxidation of organics, gas sensors, electrodes in solid-state ionic devices, molecular sieves, and solar cells due to its being chemically inert, mechanically hard, and thermally heat-resistant.[1−4] The success in many of its

technological applications depends on crystalline SnO_2 with a uniform nanosize pore structure.[5] Efforts toward the development of tin oxide nanomaterials with high sensitivity, excellent selectivity, quick response, and recovery behavior to gases has increased over the years. Tin oxide is used widely to control air pollution and to detect toxic or smelling gases at low levels in the air and in the field of domestic and industrial applications.[6] As the size of the particle decreases, the surface to volume ratio increases, which then increases the number of oxygen sites on the surfaces in these reducing gas species[6,7] and the sensitivity of nanocrystalline tin oxide.[8]

SnO_2 can be synthesized using a variety of techniques such as sol-gel,[9] hydrothermal method,[10] precipitation, carbothermal reduction, and polymeric precursor.[11] The hydrothermal method is one of the best methods to produce fine oxide powders due to its simplicity, efficiency, and environmental friendliness.[12,13] It is known that well dispersed particles have larger surface areas and smaller particle sizes, which are desired to increase the reaction sites. One of the effective methods for obtaining well dispersed and homogeneous particles is to re-crystallize them under hydrothermal treatment.[14] In most cases, metal oxide particles synthesized at room temperature readily aggregate with each other due to poor crystallinity.[15]

It was found that precipitation of metal hydroxide by direct addition of ammonium hydroxide, NH_4OH, yields a large amount of powder at the same instant. However, high surface area powders are difficult to obtain because of the irregular particle morphology, large particle size distribution, and high degree of agglomeration.[7] The little control over the particle size and shape is due to the rapid change in solution concentration and the localized, discontinuous nature of the introduction of the ammonia. The direct addition of NH_4OH to $SnCl_4$ aqueous solutions has led to non-uniform supersaturation in solution. A more uniform supersaturation is best achieved by using urea as a reagent to control the pH and to obtain a pure and dense hydrous tin oxide. The homogeneous precipitation method allows the ammonia to be mixed uniformly throughout the solution at molecular levels by thermal decomposition of urea.[7] The powder from the homogeneous precipitation method was reported to have higher surface area than those obtained from the direct precipitation method.[16]

Surfactants are used in the preparation of crystalline metal oxide in the nanoscale to control crystal growth and to provide solubility. Surfactants help to organize the small oxide crystallites into a sufficiently ordered structure to generate regular pores and low angle Bragg reflection.[17] However, some surfactants are toxic and lead to impurities in the final product and hamper the application of these nanomaterials in electronic and sensing devices.[18] The surfactants have to be removed by burning the samples at higher temperature to improve thermal stability and the purity of the mesostructure tin oxide for catalysts and electrochemistry.[4]

The purpose of the present research was to synthesize pure and high surface area tin oxide with small particle size using oleyl amine, a non-ionic surfactant, as an organic template and tin tetrachloride ($SnCl_4 \cdot 5H_2O$) as inorganic precursor via the hydrothermal method through gradual decomposition of urea as a source of OH^- ions. The effects of concentration of surfactant and urea and calcination temperature on the particle size, surface area, pore size, and particle distribution were investigated.

Experimental

Materials and reagents

The chemicals used were 70% oleyl amine ($CH_3(CH_2)_7 CH{=}CH(CH_2)_8 NH_2$) (Fluka), hydrated tin tetrachloride ($SnCl_4 \cdot 5H_2O$) (Riedel-de Haen), ultrapure water obtained from SQ-Ultra Pure Water Purification System,

99.5% ethanol (C_2H_5OH) (Systerm), and 99% urea ((NH_2)$_2$CO) (Riedel-de Haen). Sodium hydroxide (NaOH) and hydrochloric acid (HCl) were from R&M Chemicals, U.K. All the above chemicals were used without further purification.

Synthesis of tin oxide via the hydrothermal method

The mixture containing 1.5 mmol of oleyl amine ($C_{18}H_{37}N$) and 20 mL of water was placed in an ultrasonicator for 30 min. Separately, 3 mmol of SnCl$_4$· 5H$_2$O was dissolved in 10 mL of water and then added into the oleyl amine solution. The solution was stirred to ensure homogeneous mixing and 0.9 g (0.5 mol L^{-1}) of granular urea was added to this mixture. After stirring for 1 h, the resulting mixture was transferred into a Teflon-lined autoclave and heated at 100 °C for 24 h. The resulting product was filtered and washed with ethanol and water via centrifugation (25,000-30,000 rpm) to remove the NH_4^+ and Cl$^-$ ions, and dried in an oven at 100 °C for 24 h. The dried solids were ground into powder using a mortar and pestle before calcination at 600 °C for 2 h. The concentrations of surfactant and urea and calcination temperature were varied from 0.003 to 0.5 mol L^{-1}, 0.5 to 1.5 mol L^{-1}, and 600 to 800 °C, respectively.

Determination of Sn-OH concentration

The alkali neutralization method[19] was used to determine the concentration of Sn-OH groups in the sample. Generally, W g of SnO$_2$ was mixed with 50 mL of 0.05 mol L^{-1} aqueous solution of NaOH in a 100 mL conical flask. The mixture was stirred for 24 h and subsequently centrifuged. Then 10 mL of supernatant was collected and titrated against standardized 0.05 mol L^{-1} aqueous solution of HCl (A mL) using 0.1% phenolphthalein as indicator. The above procedures were repeated with a blank solution and the volume of HCl consumed for neutralization was designated as B mL. The amount of total hydroxyl group (X mmol g^{-1}) per unit grams of the tin oxide was estimated using the formula:

$$X = \frac{(B - A) \times 0.05 \times 5}{W}$$

Characterizations

FT-IR: Fourier transform infrared (FT-IR) spectroscopy analysis was conducted on the tin oxide samples using Perkin-Elmer Spectrum GX infrared spectrophotometer. A 5 mg sample was mixed with 200 mg of KBr to produce a pellet (KBr disk) under 12,000 pounds of pressure. The translucent pellet was dried at 120 °C for 24 h. FTIR spectroscopy analysis was performed in the 400-4000 cm^{-1} region.

   XRD: X-ray diffraction (XRD) was used to determine the phases present and the preferred orientation of the deposits. XRD, SIEMENS D5000 with Cu K$_\propto$($\lambda = 1.5406$ Å) was employed to obtain XRD spectra. A computer-based search and match was used for phase identification. The average crystallite size of the nanoparticle was calculated using the Scherrer formula:

$$d = \frac{K\lambda}{(\beta \cos\theta)},$$

where d is the mean crystallite size, K is the grain shape dependent constant 0.89, λ is the wavelength of the incident beam in nm, θ is the Bragg reflection angle, and β is the line broadening at half the maximum intensity in radians.

BET: The specific surface area and pore size distributions were measured by the Brunauer-Emmett-Teller (BET) method with nitrogen adsorption at 77 K using micrometrics ASAP 2000 model gas sorption analyzer. The samples were out-gassed at 200 °C for 3 h.

TEM: The size and the shape of particles were analyzed by Philips CM12, 80 kV transmission electron microscopy (TEM) system. The measurement of the particle size was performed using the analysis Docu Version 3.2 image processing software for the particle size of 300 particles from TEM micrographs. A small amount of the sample was suspended in 100% ethanol as required. A droplet of the suspension was placed on a carbon film coated 400 mesh copper grid for 3 min. The droplet should be pipetted out after large particles have settled to the bottom of the sample tube. The droplet was wiped to dryness using filter paper. The grid was placed on a filter paper lined petri dish until it could be examined.

SEM-EDX: Scanning electron microscopy (SEM) was used to study the surface morphology using a Leo Supra 50 VP operated at 10-15 kV. The sample to be analyzed was placed on double-sided tape adhered to the specimen holder. All samples must be trimmed to an appropriate size to fit in a specimen chamber and mounted on some sort of a holder. The SEM requires that specimens be conductive for the electron beam to scan the surface and coating of electrically conducting material (Au) is needed if otherwise. Energy dispersive X-ray Oxford Incha 400 operated at 15 kV was used with dimensions of around 1 μm with a sensitivity of about 0.1 wt % to detect the possible elements found on the surface of tin oxide.

TGA: Thermogravimetry analysis was carried out to determine changes in weight in relation to changes in temperature. Analysis was performed using a Perkin Elmer TGA7 model and samples were heated at the temperature range of 30 to 900 °C at the rate of 20 °C min^{-1} under flow of N_2 gas.

Results and discussion

Effect of calcination temperature

The FTIR spectra of SnO_2 at the different conditions investigated are shown in Figure 1. The peak at around 614-930 cm^{-1}, which refers to Sn-O stretching modes of Sn-O-Sn, becomes sharper as the calcination temperature increases to 800 °C. The peaks at 1384 and 1401 cm^{-1} were assigned to the NH deformation of ammonia and NH stretching vibration from the decomposition of urea.[20]

The presence of water molecules adsorbed on the surface of tin oxide during handling or OH groups stretching vibrations can be seen in the 1618-1635 cm^{-1} and 3200-3600 cm^{-1} regions.[11,21] The difference in the FTIR spectra before and after calcination is that the intensity of the bands at 1618-1635 cm^{-1} and 3200-3600 cm^{-1} has been reduced due to the removal of water during the calcination process. Upon leaving the pellet in the oven for 1 day (Figure 1c), the intensity of the peaks at 3420, 1384, and 1618 cm^{-1} was greatly reduced. The uncalcined sample (Figure 1e) shows a peak at about 532 cm^{-1}, which is attributed to the Sn-OH group. When the sample is calcined (at 600 and 800 °C), the peak at about 532 cm^{-1} disappears, which indicates that the condensation reaction occurs upon heating to produce SnO_2.[7]
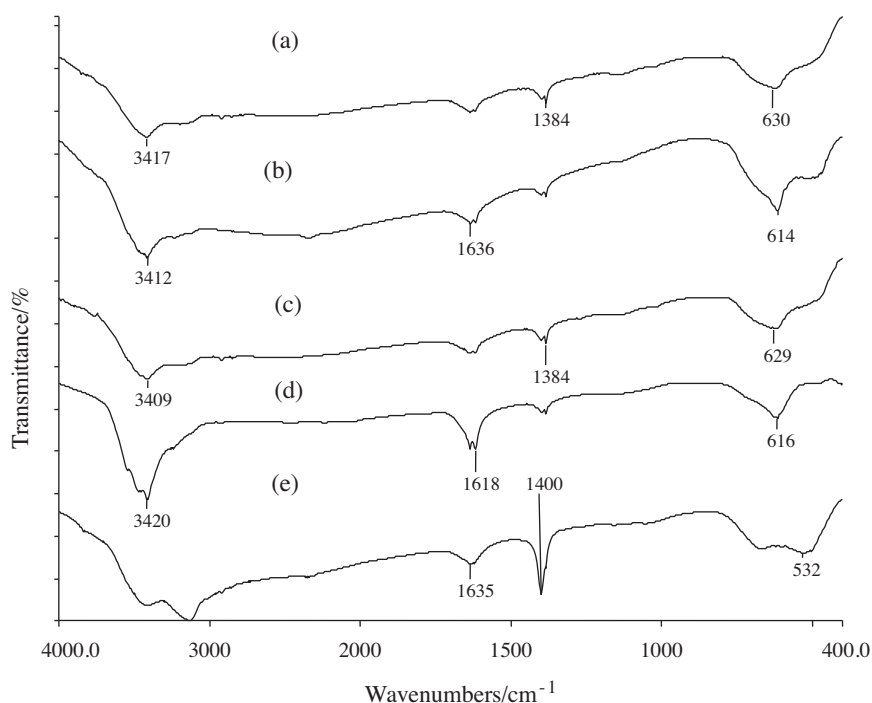
Figure 1. FTIR spectra of tin oxide samples synthesized at different calcination temperatures (a) 600 °C, (b) 800 °C, (c) calcined at 600 °C and pellet was dried in the oven at 100 °C, (d) calcined at 600 °C and pellet was left at room temperature (e), not calcined.

The XRD pattern in Figure 2 was recorded in the region of 2θ value of 20-80° to investigate the effect of calcination temperature on the tin oxide structure. The uncalcined sample showed no diffraction peaks, indicating that the uncalcined sample is amorphous. This can be explained due to the presence of the surfactant used. After calcination at 600 °C, peaks due to SnO_2 were located at 2θ values of 26.5, 33.9, 37.9, 51.8, 54.7, 61.9 and 65.9° for reflection planes of (1 1 0), (1 0 1), (2 0 0), (2 1 1), (2 2 0), (3 1 0) and (3 0 1), respectively of the tetragonal lattice of tin oxide. The corresponding lattice constant is $\sim$ 4.73650 Å, which was compared with the standard reported data (JCPDS File No.01-070-6153). The intensity of these reflections planes increased with increasing calcination temperature, 800 °C, whereas the 2θ values of these diffraction lines remained practically constant.[22] No obvious reflection peaks from the impurities, such as unreacted Sn or other tin oxides such as SnO, were detected, indicating high purity of the products.[23] The average particle size is 9.92 nm, as calculated by the Scherrer equation, using the half width of intense (211) reflection plane. The broad peak in Figure 2a indicates a small crystallite domain size. The broadenings of the peaks decrease with the increase in heat treatment temperatures, suggesting the growth of SnO_2 crystallites size.[24]

The BET results displayed in Table 1 show that the surface area decreases, while the average pore diameter and the crystallite size increase as the calcination temperature increases due to elimination of ammonia, physically adsorbed water, and chemically bonded water trapped in the powder.[7] At optimum conditions (precursor to surfactant ratio of 1:0.02, concentration of urea of 0.5 M, and calcination temperature of 600 °C), the surface area of tin oxide powders is 31.82 m^2 g^{-1}, which is higher than those reported for other SnO_2 powders (15 m^2 g^{-1}) prepared by precipitation.[7] As calcination involves condensation of surface hydroxyl

307

groups, the uncalcined sample has a higher surface area because of the presence of hydroxyl groups and surfactant.
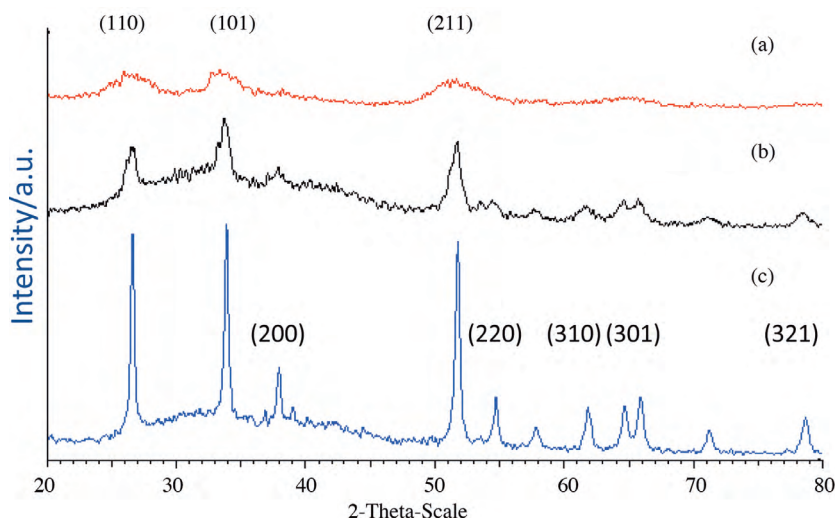

Figure 2. XRD diffractograms of tin oxide (a) not calcined, and calcined at: (b) 600 °C, (c) 800 °C.

Table 1. Effect of calcination temperature on particle size, surface area, and average diameter pore size of the tin oxide.

Sample	Crystallite size/nm	Surface area	Average pore
	by XRD	(m^2 g^{-1})	Diameter/nm
Uncalcinated	5.11	141.56	2.38
Calcinated at 600 °C	9.92	31.82	10.02
Calcinated at 800 °C	21.36	19.54	17.58

Effect of calcination temperature on morphology

Figure 3 shows SEM micrographs of the synthesized tin oxide. Figure 3a shows a sponge-like distribution of particles when the sample was not calcined. Figure 3b shows a rough surface with many projecting particles when calcined at 600 °C for 2 h. However, the mesostructure of the powder calcined at 800 °C for 2 h shows a compact arrangement of spherical and uniform tin oxide particles as shown in Figure 3c.

The energy dispersion X-ray (EDX) analyses results are displayed in Table 2; they were used to confirm the composition of the tin oxide samples. The results obtained are confirmed by the TGA analysis whereby the release of carbon dioxide is detected at 240, 670, and 890 °C. The residual carbon may arise from the ethanol used during washing for the uncalcined sample[24] and could also be due to the double-sided tape used to place the sample on its holder. For the calcined sample the presence of carbon is more likely due to the latter cause. Surfactant has no influence on the final composition because it is completely burned off during the calcination process[25] since the melting point of oleyl amine is 17-27 °C. SEM/EDX analysis shows that no trace of Cl$^-$ ions was detected in the powders after calcination, which indicates relatively pure samples despite the use of tin(IV) chloride. This result is consistent with that of the FTIR spectra (Figure 1), as no peak at 435 cm^{-1} due to Sn-Cl vibrations was observed.[26]
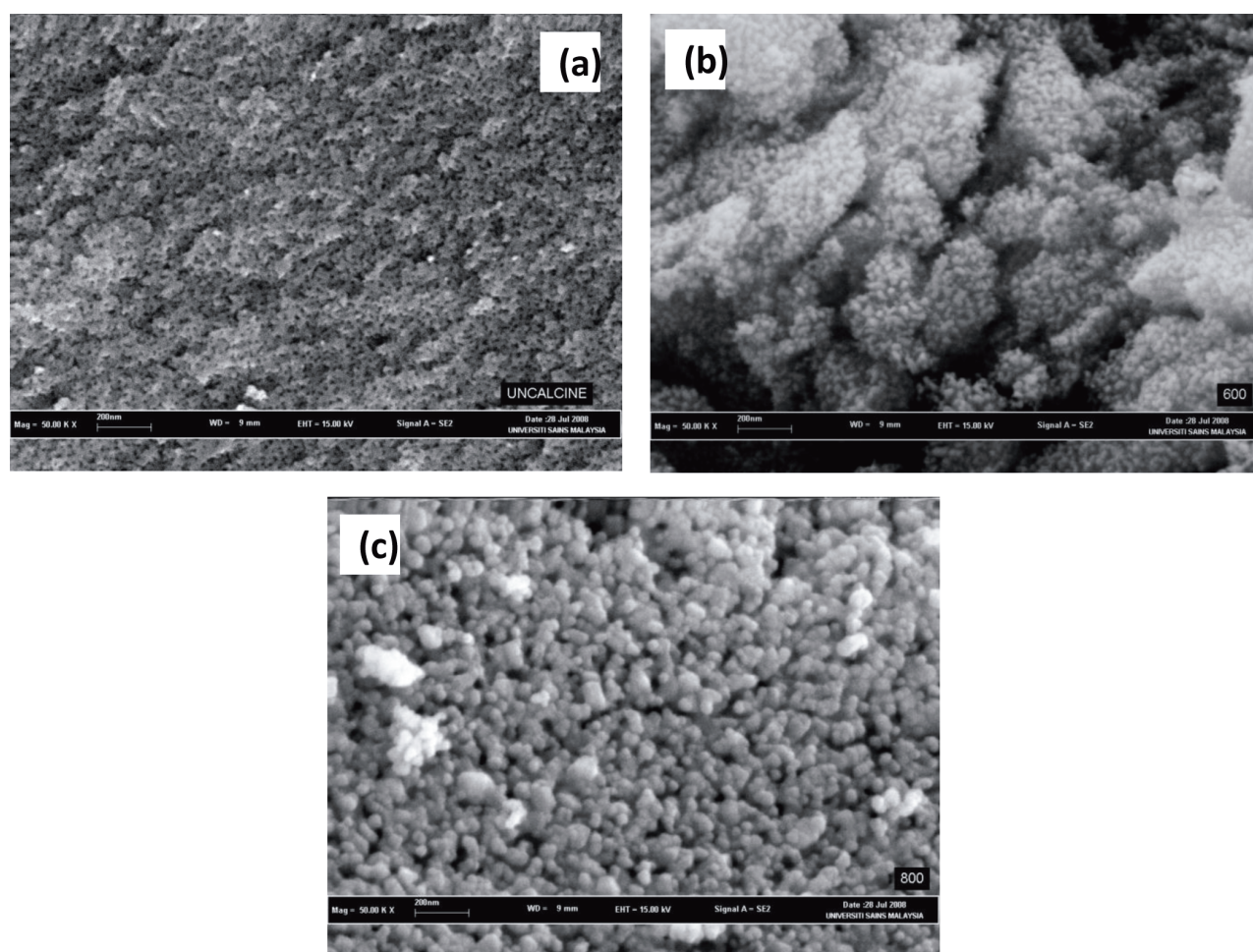
Figure 3. SEM images of tin oxide nanoparticles (a) uncalcined sample, (b) calcined at 600 °C, (c) calcined at 800 °C.

Table 2. Percentage of atomic weight based on EDX analysis for each element found in the sample of tin oxide before and after calcinations.

Elements	Before calcination atomic %			After calcination atomic %		
	Area 1	Area 2	Average	Area 1	Area 2	Average
C	12.81	7.54	10.18	12.43	3.66	8.05
O	59.41	62.17	60.79	58.07	71.46	64.77
Sn	22.09	27.28	24.69	29.01	24.88	26.95
Cl	5.69	7.01	6.35	-	-	-

Effect of calcination temperature on particle distribution

Based on the TEM images in Figure 4 of the as-synthesized tin oxide nanoparticles at different calcination temperatures, the optimum calcination temperature was found to be at 600 °C because more agglomerates were observed following calcination at higher temperature (Figure 4 c) .
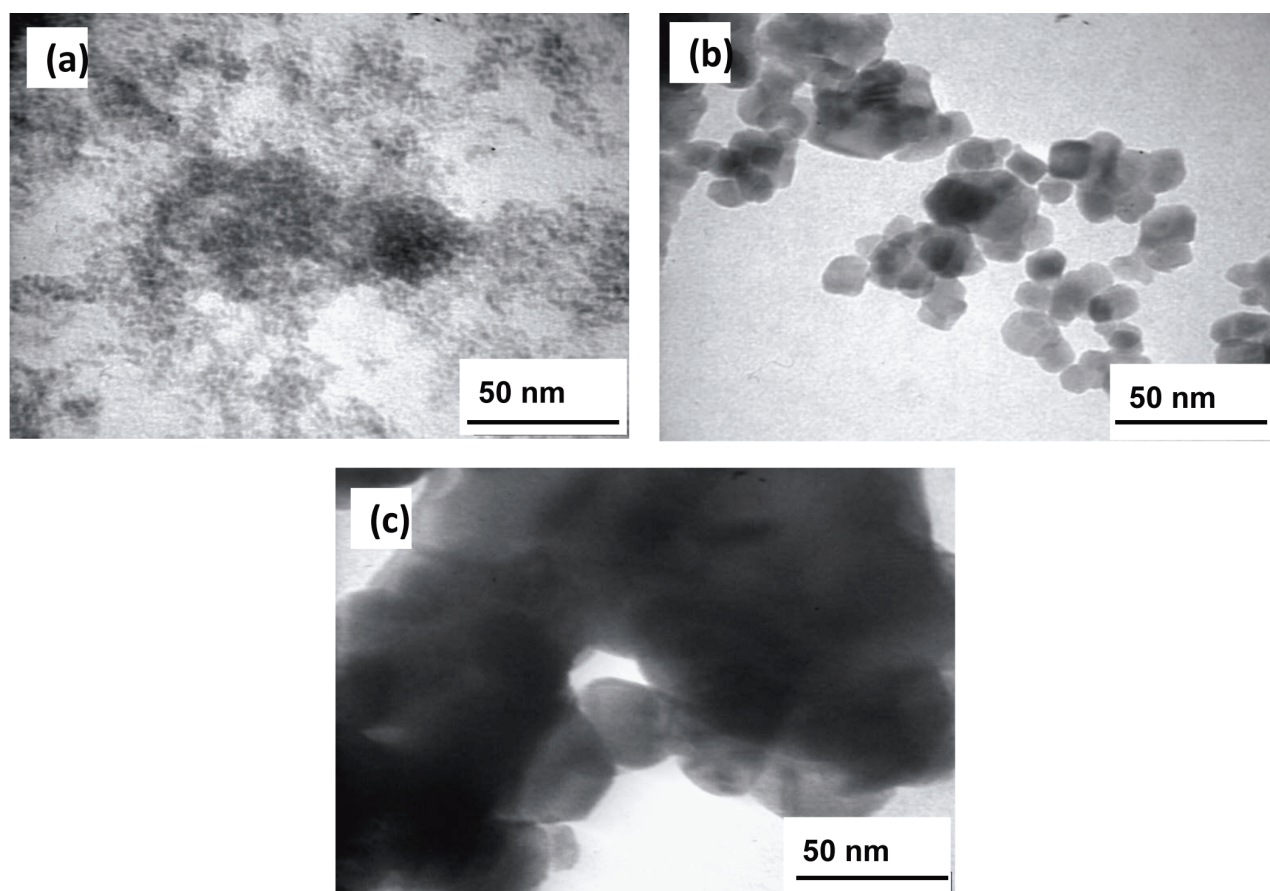
Figure 4. TEM images of tin oxide nanoparticles (a) uncalcined sample, (b) calcined at 600 $^\circ$C, (c) calcined at 800 $^\circ$C (scale bar: 50 nm).

Thermal analysis (Figure 5) shows that the uncalcined sample undergoes greater weight % loss due to the decomposition of carbonates and surfactant, and evaporation of physically adsorbed water chemically bonded water and ethanol at the range from 35 to 890 $^\circ$C than the sample calcined at 600 $^\circ$C and 800 $^\circ$C. This shows that the sample dried at 100 $^\circ$C for 24 h still has a reasonable amount of water trapped in the sample when it is not calcined.

It was reported by Severin and Abdel-Fattah[17] that calcination at high temperature such as 800 $^\circ$C may lead to extensive sintering and condensation of the surface hydroxyl groups. Little weight loss in the TGA curve is observed at temperatures above 600 $^\circ$C, indicating the completion of any reactions involving a weight change.[7]

As the calcination temperature increases, the percentage of weight loss decreases, indicating the complete removal of oleyl amine. The calcination process aimed to remove the organic impurities and results in dehydroxylation of Sn-OH groups. This explains why the sample should be calcined at a higher temperature. At low calcination temperatures, the OH groups were still present at the surface and at the interior of SnO particles. The OH groups can be removed at higher calcination temperature.[27]

Effect of concentration of urea

Slow addition of ammonium hydroxide through decomposition of urea improves the condensation of free Sn-OH and Sn-Cl species during the synthesis of nanoparticles, leading to a more fully condensed tin oxide framework. As shown in Figure 6, the number of active Sn-OH sites available to promote crystallization of tin oxide lattices decreased at higher urea concentrations. [28]
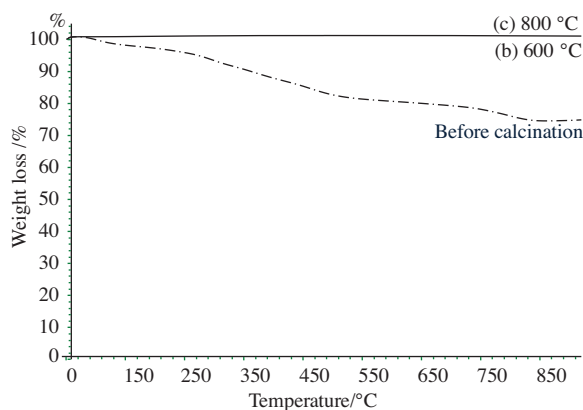

Figure 5. TGA curves of tin oxide samples heated to 30-900 $^{\circ}$C at a rate of 20 $^{\circ}$C min^{-1} (a) before calcination, (b) calcination at 600 $^{\circ}$C, (c) calcination at 800 $^{\circ}$C.
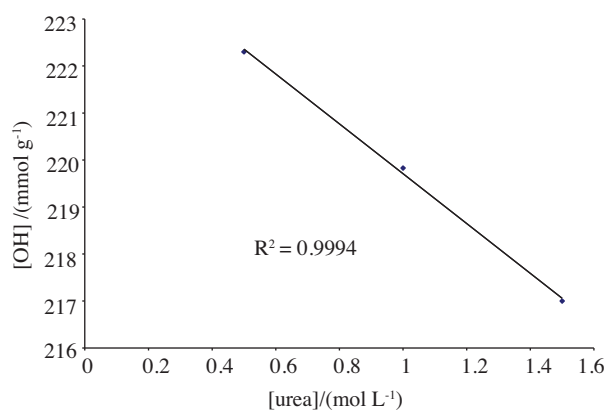
Figure 6. Concentration of hydroxyl groups per unit gram of tin oxide as a function of concentration of urea.

Figure 7 shows the TEM images of tin oxide synthesized at 0.5, 1.0, and 1.5 mol L^{-1} of urea. The 0.5 mol L^{-1} urea used gives rise to well dispersed particles and smaller particle size due to slow hydrolysis and condensation reaction. However, the particles tend to agglomerate when 1.5 mol L^{-1} of urea is used. The particle size increased with the increase in the concentration of urea at 1.5 mol L^{-1}. The elevated pH value created a high super saturation level due to the large concentration of hydroxyl ions in solution, resulting in an extremely fast nucleation process generating tiny nuclei. [29] The tiny nuclei that form will dissolve and re-precipitate on the growing secondary particles through Ostwald ripening. [30] The TEM results were proven with XRD analyses and the crystallite sizes calculated by Scherrer equation were 9.92, 12.00, and 12.39 nm at 0.5, 1.0, and 1.5 mol L^{-1} of urea, respectively.

Effect of concentration of surfactant to metal precursor

The addition of surfactant leads to a very narrow size distribution of the particles up to 5.36 nm at below CMC of oleyl amine. The oleyl amine (non-ionic surfactant) might coordinate to the Sn ions and slow down the hydrolysis and condensation of the precursor, making the nucleation complete at the early stage of the sol-gel process and inhibiting crystal growth. According to Zhang and Gao, [24] in the absence of oleyl amine, the nucleation process is comparatively slow, which results in a broad size distribution of the SnO$_2$ nanocrystallites.

Figure 8 shows that as the doses of surfactant increases from 1:0.02 to 1:3 the particle size increases from 5.36 to 51.2 nm. The particles tend to agglomerate with the increase in surfactant's concentration. Therefore the amount of surfactant added is crucial in synthesizing tin oxide with well dispersed particles. The surfactants

create their own interface and form micelles at critical micelle concentration.[31] Under these conditions there would be micelle formation in the bulk phase and less surfactant-coated nanoparticles formed.[32] When the surfactant forms micelles, the latter are not effective in dispersing the particles compared to when they are individually apart, which leads to an increase in particle size.
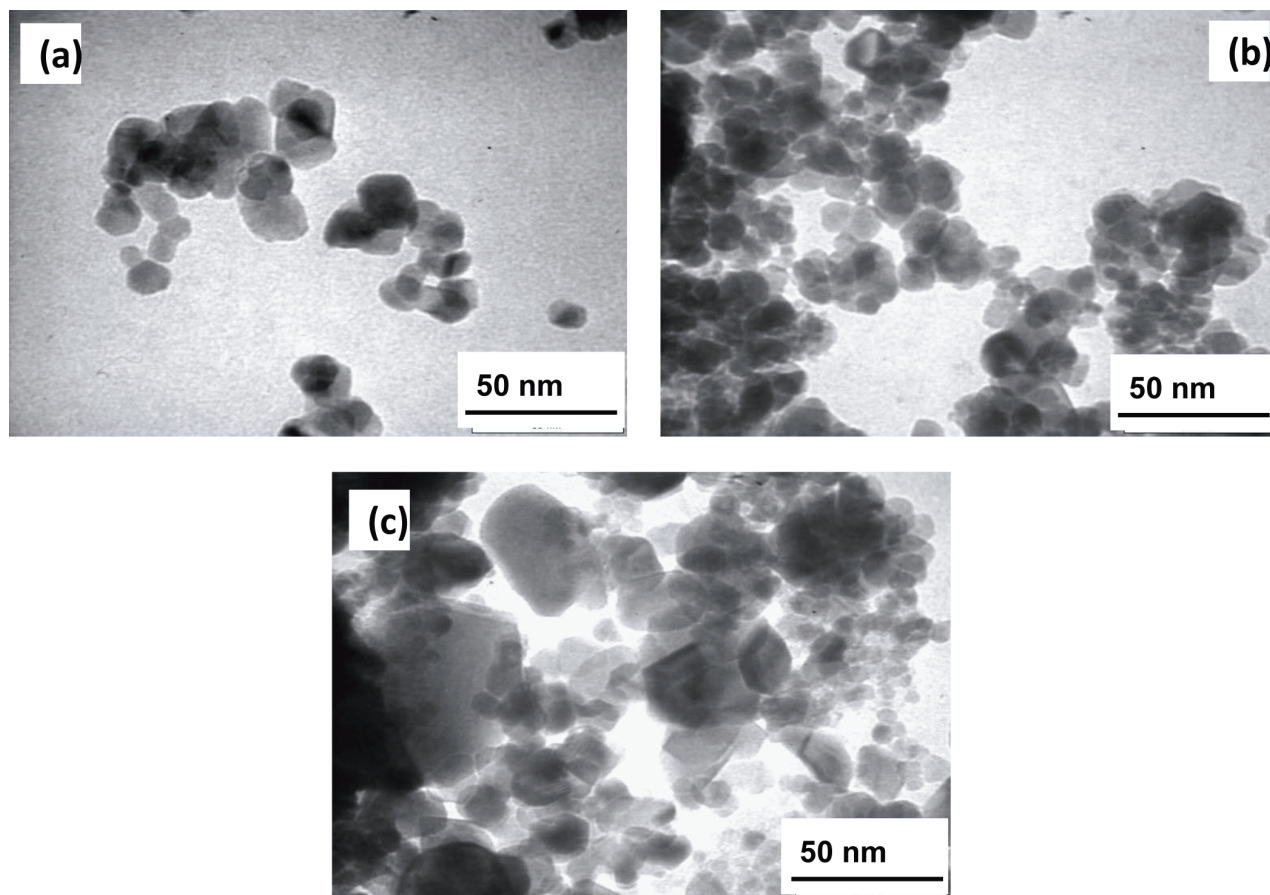

Figure 7. TEM images of as-synthesized nanostructured tin oxide at different concentration of urea (a) 0.5 mol L^{-1}, (b) 1.0 mol L^{-1}, (c) 1.5 mol L^{-1} (scale bar: 50 nm).
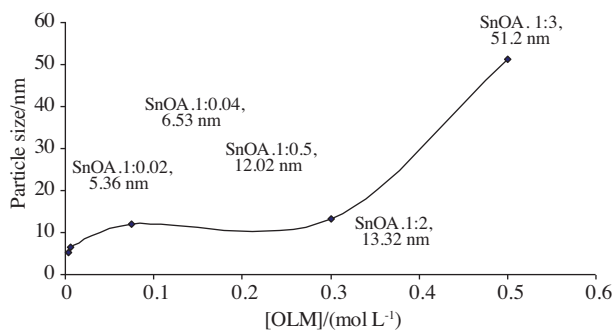

Figure 8. Effect of concentration of surfactant on particle size under hydrothermal conditions.

Conclusion

Tin oxide nanoparticles were prepared using hydrous tin chloride ($SnCl_4 \cdot 5H_2O$) as inorganic precursor via the hydrothermal method in the presence of oleyl amine and urea as the non-ionic surfactant and alkali source, respectively. The tin oxides with crystallites sizes of 9.92 nm and surface area of $31.82 \, m^2 \, g^{-1}$ were successfully synthesized by using $0.5 \, mol \, L^{-1}$ urea and calcined at $600 \, °C$. It was found that the concentration of urea was proportional to the condensation of free Sn-OH and particle size. The crystallites' size and surface area and pore diameter of nanoparticles were found to be dependent on calcination temperature and concentration of urea. The crystallites' size and pore diameter increase while surface area decreases with increases in temperature. Surfactant plays an important role in controlling the particle size. The addition of surfactant leads to small particle size up to 5.36 nm at below CMC of oleyl amine, while particle size of SnO_2 as reported in literature in the presence of anionic surfactant (SDS), cationic surfactant (CTABr), and nononic surfactant (PEG) under hydrothermal condition was reported to be 8, 11, and 13 nm, respectively, which is greater than our findings in the presence of oleyl amine.[33] However, particle size increases when surfactant concentration is above CMC due to micelle formation where particles are agglomerated to each other to form bigger particles.

Acknowledgements

References

1. Chopra, K.; Major, S.; Panda, D. *Thin Solid Films.* **1983**, *102*, 1-46.

2. Williams, D. E. *In Solid State Gas Sensors*, Moseley, P. T.; Tofield, B. C., Eds.; Adam Hilger, Bristol, 1987.

3. Shukla, S.; Seal, S. *J. Meteor.* **2002**, *54*, 35-38.

4. Wang, Y. D.; Ma, C. L.; Sun, X. D.; Li, H. D. *Inorg. Chem. Commun.* **2001**, *4*, 223-226.

5. Qi, L.; Ma, J.; Cheng, H.; Zhao, Z. *Langmuir.* **1998**, *14*, 2579-2581.

6. Vaezi, M. R.; Sadrnezhaad, S. K. *Mater. Sci. Eng. B-Solid.* **2007**, *140*, 73-80.

7. Song, K. C. ; Kang, Y. *Mater. Lett.* **2000**, *42*, 283-289.

8. Shukla, S.; Seal, I. S. *Encyclopedia of Nanoscience and Nanotechnology,* American Scientific Publisher, California, 2003.

9. Adnan, R.; Razana, N. A.; Rahman, I. A.; Farrukh, M. A. *J. Chin. Chem. Soc.* **2010**, *57*, 222-229.

10. Farrukh, M. A.; Heng, B.-T.; Adnan, R. *Turk. J. Chem.* **2010**, *34*, 537-550.

11. Ibarguen, A. C.; Mosquera, A.; Parra, R.; Castro, M. S.; Rodríguez-Páez, J. E. *Mater. Chem. Phys.* **2007**, *101*, 433-440.

12. Sōmita, S.; Roy, R. *Bull. Mater. Sci.* **2000**, *23*, 453-460.

13. Zhu, H.; Wang, Y.; Wang, N.; Li, Y.; Yang, J. *Mater. Lett.* **2004**, *58*, 2631-2634.

14. Wu, Q. L.; Xiang, L.; Jin, Y. *Powder Technol.* **2006**, *165*, 100-104.

15. Yan, H.; Zhang, X.-H.; Wu, J.-M.; Wei, L.-Q.; Liu, X.-G.; Xu, B.-S. *Powder Technol.* **2008**, *188*, 128-132.

16. Acarbas, Ö.; Suvacı, E.; Doğan, A. *Ceram. Int.* **2007**, *33*, 537-542.

17. Severin, K. G.; Abdel-Fattah, T. M. *Chem. Commun.* **1998**, *14*, 1471-1472.

18. Niederberger, M.; Garnweitner, G.; Pinna, N.; Neri, G. *Prog. Solid State Chem.* **2005**, *33*, 59-70.

19. Jeffry, G. H.; Bassett, J.; Mendhan, J.; Denney, R. C. *Vogel's Textbook of Quantitative Chemical Analysis,* Longman Group, London, 1998.

20. Yu, J.; Zhao, L.; Cheng, B. *J. Solid State Chem.* **2006**, *179*, 226-232.

21. Popescu, D. A.; Verduraz, F. B. *Catal. Today* **2001**, *70*, 139-154.

22. Liu, H.; Ma, Z.; Chu, Y.; Sun, W. *Colloids Surf. A,* **2006**, *287*, 10-15.

23. Kim H. W.; Shim S. H. *J. Alloys Compd.* **2006**, *426* 286-289.

24. Zhang, J.; Gao, L. *J. Solid State Chem.* **2004**, *177*, 1425-1430.

25. Hasab, G. M.; Seyyed, E. S. A.; Badiei, A. *J. Magn. Magn. Mater*. **2007**, *316*, e13-e15.

26. Ocana, M.; Serna, C. J.; Garcia-Ramos, J. V.; Matijevic, E. *Solid State Ionics.* **1993**, *63*, 170-177.

27. Krishnakumar, T.; Pinna, N.; Prasanna, K. K.; Perumal, K.; Jayaprakash, R. *Mater. Lett.* **2008**, *62*, 3437-3440.

28. Scott, R. W. J.; Mamak, M.; Kwong, K.; Coombs, N.; Ozin, G. A. *J. Mater. Chem.* **2003**, *13*, 1406-1412.

29. Yan, T.; Wang, X.; Long, J.; Liu, P.; Fu, X.; Zhang, G.; Fu, X. *J. Colloid Interface Sci.* **2008**, *325*, 425-431.

30. Brinker, C. J.; Scherer, G. W. *Sol-Gel Science: The Physics and Chemistry of Sol- Gel Processing*, Academic Press Inc., San Diego, 1990.

31. Muherei, M. A.; Junin, R. *Modern Applied Science* **2008**, *2,* 3-12.

32. Bryleva, E. Y.; Vodolazkaya, N. A.; Mchedlov-Petrossyan, N.O.; Samokhina, L. V.; Matveevskaya, N. A.; Tolmachev, A.V. *J. Colloid and Interface Sci.* **2007**, *316*, 712- 722.

33. Gnanam, S.; Rajendran, V. *Digest J. Nanomater. Biostructure.* **2010**, *5*, 623-628